Yamochi, T., Urano, T., Furukawa, K., Kwabi-Addo, B., Gold, D. L., Sekido, Y., Huang, T. H., and Issa, J. P. (2008) Gene silencing in cancer by histone H3 lysine 27 trimethylation independent of promoter DNA methylation. *Nat. Genet.* **40,** 741–750

30. Kondo, Y., Shen, L., Yan, P. S., Huang, T. H., and Issa, J. P. (2004) Chromatin immunoprecipitation microarrays for identification of genes silenced by histone H3 lysine 9 methylation. *Proc. Natl. Acad. Sci. U.S.A.* **101,** 7398–7403
31. Gao, W., Kondo, Y., Shen, L., Shimizu, Y., Sano, T., Yamao, K., Natsume, A., Goto, Y., Ito, M., Murakami, H., Osada, H., Zhang, J., Issa, J. P., and Sekido, Y. (2008) Variable DNA methylation patterns associated with progression of disease in hepatocellular carcinomas. *Carcinogenesis* **29,** 1901–1910
32. Bronstein, J. M., Tiwari-Woodruff, S., Buznikov, A. G., and Stevens, D. B. (2000) Involvement of OSP/claudin11 in oligodendrocyte membrane interactions: role in biology and disease. *J. Neurosci. Res.* **59,** 706–711
33. Adams, B., Dörfler, P., Aguzzi, A., Kozmik, Z., Urbánek, P., Maurer-Fogy, I., and Busslinger, M. (1992) Pax-5 encodes the transcription factor BSAP and is expressed in B lymphocytes, the developing CNS, and adult testis. *Genes Dev.* **6,** 1589–1607
34. Farah, M. H., Olson, J. M., Sucic, H. B., Hume, R. I., Tapscott, S. J., and Turner, D. L. (2000) Generation of neurons by transient expression of neural bHLH proteins in mammalian cells. *Development* **127,** 693–702
35. Letzen, B. S., Liu, C., Thakor, N. V., Gearhart, J. D., All, A. H., and Kerr, C. L. (2010) MicroRNA expression profiling of oligodendrocyte differentiation from human embryonic stem cells. *PLoS ONE* **5,** e10480
36. Hirabayashi, Y., and Gotoh, Y. (2010) Epigenetic control of neural precursor cell fate during development. *Nat. Rev. Neurosci.* **11,** 377–388
37. Suzuki, Y., Yamashita, R., Nakai, K., and Sugano, S. (2002) DBTSS: DataBase of human Transcriptional Start Sites and full-length cDNAs. *Nucleic Acids Res.* **30,** 328–331
38. Morita, K., Sasaki, H., Fujimoto, K., Furuse, M., and Tsukita, S. (1999) Claudin11/OSP-based tight junctions of myelin sheaths in brain and Sertoli cells in testis. *J. Cell Biol.* **145,** 579–588
39. He, J., Mokhtari, K., Sanson, M., Marie, Y., Kujas, M., Huguet, S., Leuraud, P., Capelle, L., Delattre, J. Y., Poirier, J., and Hoang-Xuan, K. (2001) Glioblastomas with an oligodendroglial component: a pathological and molecular study. *J. Neuropathol. Exp. Neurol.* **60,** 863–871
40. Homma, T., Fukushima, T., Vaccarella, S., Yonekawa, Y., Di Patre, P. L., Franceschi, S., and Ohgaki, H. (2006) Correlation among pathology, genotype, and patient outcomes in glioblastoma. *J. Neuropathol. Exp. Neurol.* **65,** 846–854
41. Woo, C. J., Kharchenko, P. V., Daheron, L., Park, P. J., and Kingston, R. E. (2010) A region of the human HOXD cluster that confers polycomb group responsiveness. *Cell* **140,** 99–110
42. Yamagishi, M., Nakano, K., Miyake, A., Yamochi, T., Kagami, Y., Tsutsumi, A., Matsuda, Y., Sato-Otsubo, A., Muto, S., Utsunomiya, A., Yamaguchi, K., Uchimaru, K., Ogawa, S., and Watanabe, T. (2012) Polycomb-mediated loss of miR-31 activates NIK-dependent NF-κB pathway in adult T cell leukemia and other cancers. *Cancer Cell* **21,** 121–135
43. Cedar, H., and Bergman, Y. (2009) Linking DNA methylation and histone modification: patterns and paradigms. *Nat. Rev. Genet.* **10,** 295–304
44. Dugas, J. C., Cuellar, T. L., Scholze, A., Ason, B., Ibrahim, A., Emery, B., Zamanian, J. L., Foo, L. C., McManus, M. T., and Barres, B. A. (2010) Dicer1 and miR-219 are required for normal oligodendrocyte differentiation and myelination. *Neuron* **65,** 597–611
45. Shin, D., Shin, J. Y., McManus, M. T., Ptácek, L. J., and Fu, Y. H. (2009) Dicer ablation in oligodendrocytes provokes neuronal impairment in mice. *Ann. Neurol.* **66,** 843–857
46. Kasinski, A. L., and Slack, F. J. (2011) MicroRNAs en route to the clinic: progress in validating and targeting microRNAs for cancer therapy. *Nat. Rev. Cancer* **11,** 849–864
47. Agarwal, R., Mori, Y., Cheng, Y., Jin, Z., Olaru, A. V., Hamilton, J. P., David, S., Selaru, F. M., Yang, J., Abraham, J. M., Montgomery, E., Morin, P. J., and Meltzer, S. J. (2009) Silencing of claudin11 is associated with increased invasiveness of gastric cancer cells. *PLoS ONE* **4,** e8002
48. Awsare, N. S., Martin, T. A., Haynes, M. D., Matthews, P. N., and Jiang, W. G. (2011) Claudin11 decreases the invasiveness of bladder cancer cells. *Oncol. Rep.* **25,** 1503–1509
49. Soini, Y., Rauramaa, T., Alafuzoff, I., Sandell, P. J., and Kärjä, V. (2010) Claudins 1, 11, and twist in meningiomas. *Histopathology* **56,** 821–824
50. Garraway, L. A., and Sellers, W. R. (2006) Lineage dependency and lineage-survival oncogenes in human cancer. *Nat. Rev. Cancer* **6,** 593–602

doi: 10.1111/j.1472-8206.2012.01056.x

ORIGINAL ARTICLE

Thymoquinone as an anticancer agent: evidence from inhibition of cancer cells viability and invasion in vitro and tumor growth *in vivo*

Samir Attoub[a]*, Olivier Sperandio[b], Haider Raza[c], Kholoud Arafat[a], Suhail Al-Salam[d], Mahmood Ahmed Al Sultan[a], Maha Al Safi[a], Takashi Takahashi[e] and Abdu Adem[a]

[a]*Department of Pharmacology & Therapeutics, Faculty of Medicine & Health Sciences, United Arab Emirates University, PO Box: 17666, Al Ain, United Arab Emirates*

[b]*INSERM UMR-S973/MTi, Université Paris Diderot, Bâtiment Lamarck, 35 Rue Hélène Brion, 75205 Paris Cedex 13, France*

[c]*Department of Biochemistry, Faculty of Medicine & Health Sciences, United Arab Emirates University, PO Box 17666, Al Ain, United Arab Emirates*

[d]*Department of Pathology,Faculty of Medicine & Health Sciences, UAE University, PO Box 17666, Al Ain, United Arab Emirates*

[e]*Division of Molecular Carcinogenesis, Center for Neurological Diseases and Cancer, Nagoya University Graduate School of Medicine, 65 Tsurumai-cho, Showa-ku, Nagoya, 466-8550, Japan*

Keywords
DNA damage,
invasion,
lung & breast cancer,
thymoquinone,
tumor growth,
viability

Received 11 March 2012;
revised 9 May 2012;
accepted 4 June 2012

*Correspondence and reprints:
samir.attoub@uaeu.ac.ae

ABSTRACT

Phytochemical compounds are emerging as a new generation of anticancer agents with limited toxicity in cancer patients. The purpose of this study was to investigate the potential impact of thymoquinone (TQ), the major constituent of black seed, on survival, invasion of cancer cells in vitro, and tumor growth *in vivo*. Exposure of cells derived from lung (LNM35), liver (HepG2), colon (HT29), melanoma (MDA-MB-435), and breast (MDA-MB-231 and MCF-7) tumors to increasing TQ concentrations resulted in a significant inhibition of viability through the inhibition of Akt phosphorylation leading to DNA damage and activation of the mitochondrial-signaling proapoptotic pathway. We provide evidence that TQ at non-toxic concentrations inhibited the invasive potential of LNM35, MDA-MB-231, and MDA-MB231-1833 cancer cells. Moreover, we demonstrate that TQ synergizes with DNA-damaging agent cisplatin to inhibit cellular viability. The anticancer activity of thymoquinone was also investigated in athymic mice inoculated with the LNM35 lung cells. Administration of TQ (10 mg/kg/i.p.) for 18 days inhibited the LNM35 tumor growth by 39% ($P < 0.05$). Tumor growth inhibition was associated with significant increase in the activated caspase-3. The *in silico* target identification suggests several potential targets of TQ mainly HDAC2 proteins and the 15-hydroxyprostaglandin dehydrogenase. In this context, we demonstrated that TQ treatment resulted in a significant inhibition of HDAC2 proteins. In view of the available experimental findings, we contend that thymoquinone and/or its analogues may have clinical potential as an anticancer agent alone or in combination with chemotherapeutic drugs such as cisplatin.

INTRODUCTION

Cancer is a leading cause of death worldwide and remains a therapeutic enigma. Among different forms of cancer, lung cancer is the most common with the highest mortality rate, and colorectal cancer is the second cause of cancer-related death after lung cancer in men and breast cancer in women. Hepatocellular carcinoma is also a common cancer in Asia and Africa and one of the most common causes of cancer-related mortality worldwide, accounting for about half a million deaths annually [1]. Despite advances in molecular biology of cancer, improved diagnosis, and new targeted therapies, the cure of lung, breast, and colon cancer remain elusive. To improve the survival of cancer patients, we need to develop new cytotoxic compounds and make use of selective molecular targeting anticancer drugs.

Over recent years, growing interest in phytochemical compounds with anticancer potential has been observed stimulating more in vitro and preclinical screening of these compounds. Thymoquinone (TQ), the most abundant constituent of black seed (*Nigella Sativa*), has been shown to exert anti-inflammatory, anti-oxidant, and antineoplastic effects both in vitro and *in vivo* [2,3]. TQ has been shown to inhibit cellular proliferation and induce apoptosis in human colon, breast, brain, pancreatic, and ovarian cancer cell lines [3–6]. The numerous reports on the protective effect of thymoquinone against drug-induced toxicity suggest a possible role of thymoquinone as an adjuvant in improving the quality of life of cancer patients [3]. In this study, we investigated the impact of thymoquinone on human cancer cell survival, and invasion in vitro and tumor xenograft growth *in vivo*. Our results showed a dramatic anticancer effect of TQ on a variety of tumor cells under in vitro as well as on lung tumor growth *in vivo*. We have also hypothesized functional targets that may potentially be affected by TQ using *in silico*-based protein data bank.

MATERIALS AND METHODS

Cell culture and reagents

Human lung cancer cells LNM35 (NSCLC) [7] were maintained in RPMI 1640 (Invitrogen, Paisley, UK); human hepatoma cells HepG2, human colorectal cancer cells HT29, human mammary adenocarcinoma cells (MCF-7, MDA-MB-231, and MDA-MB-213-1833), and human melanoma MDA-MB-435 were maintained in DMEM (Invitrogen). All media were supplemented with 10% fetal bovine serum (Roche Molecular Biochemicals, Meylan, France). Thymoquinone was purchased from Sigma-Aldrich (Saint-Quentin Fallavier, France).

Primary antibodies were purchased from the following manufacturers: polyclonal antibodies for cytochrome *c*, poly (ADP-ribose) polymerase (PARP), and HDAC2 (Santa Cruz, CA, USA), Bcl-2, phosphor-Akt (Cellular Signaling Technology, Beverly, MA, USA), phospho-histone H2a.X (Millipore, Hayward, CA, USA), and monoclonal rat anti-mouse CD31 antibody (BD Pharmingen, San Jose, CA, USA). The secondary antibodies were goat anti-rat antibody (Sigma, Saint Louis, MO, USA) and rabbit anti-mouse antibody (Dako, Copenhagen, Denmark). Signal Stain Cleaved Caspase-3 (Asp175) IHC detection kit was purchased from Cellular Signaling Technology).

Cellular viability

Cells were seeded at 5000 cells/well in 96-well plate. After 24 h, cells were treated for another 24 h with increasing concentrations of thymoquinone (1–100 μM) in triplicates. Control cultures were treated with 0.1% DMSO. The effect of thymoquinone on cell viability was determined using a CellTiter-Glo luminescent cell viability assay (Promega Corporation, Madison, WI, USA), based on quantification of ATP, which signals the presence of metabolically active cells. Luminescent signal was measured using GLOMAX Luminometer system. The data were presented as proportional viability (%) by comparing the treated group with the untreated cells, the viability of which is considered as 100%.

Caspase-3/7 activity

Cells were seeded at a density of 5000 cells/well into 96-well plate and treated with 10 μM of thymoquinone (HepG2) and with 100 μM of thymoquinone for 24 h (LNM35), in triplicate assays. Caspase-3/7 activity was measured using a luminescent Caspase-Glo 3/7 assay kit following manufacturer's instructions (Promega Corporation). Caspase reagent was added, and the plate was mixed using an orbital shaker and incubated for 2.5 h at room temperature. Luminescence was measured using a GLOMAX Luminometer system (Promega, Madison, WI, USA).

Expression of apoptotic and DNA damage protein members

LNM35 and MDA-MB-231 cells were seeded in 100 mm dishes at 3×10^6 cells/dish for 24 h and with

increasing concentrations of thymoquinone (1–50 μM) for 30 min, 2, 6, and 24 h. Total cellular proteins were isolated using RIPA buffer (25 mM Tris–HCl pH 7.6, 1% nonidet P-40, 1% sodium deoxycholate, 0.1% SDS, 0.5% protease inhibitors cocktail, 1% PMSF, 1% phosphatase inhibitors cocktail) from control and treated cells. The whole cell lysate was recovered by centrifugation at 23 000 g for 20 min at 4 °C to remove insoluble material, and 50 μg of protein was separated by a 10% SDS gel for phospho-Akt and HDAC2 and 12% SDS gel for Anti-phospho-Histone H_2aX. After electrophoresis, the proteins were transferred on a nitrocellulose membrane, blocked with 5% non-fat milk and probed with $pSer^{473}$-Akt (1 : 1000), H_2aX (1 : 500), HDAC2 (1 : 200), and β-actin (1 : 1000) antibodies overnight at 4 °C. The blot was washed, exposed to horseradish peroxidase (HRP)-conjugated secondary antibodies, and visualized using the ECL system (Santa Cruz).

For the expression of cytochrome *c*, PARP, and Bcl-2, the cells were seeded in 100 mm dishes at 3×10^6 cells/dish and treated with 10 μM of thymoquinone for 6 and 24 h. After, cells were harvested, washed with PBS (pH 7.4), and homogenized in mitochondrial isolation H-medium buffer (70 mM sucrose, 220 mM mannitol, 2.5 mM HEPES, 2 mM EDTA) and 0.1 mM phenylmethylsulfonylfluoride at 4 °C. Mitochondria and postmitochondrial supernatants (PMS) were prepared by centrifugation, and the purity of the mitochondrial fraction was ascertained by assaying for organelle-specific marker enzymes as described previously [8]. Mitochondrial preparations containing <3% cross-contamination were used in experiments. Proteins (50 μg) from mitochondria and PMS were separated on 12% SDS-PAGE and electrophoretically transferred onto nitrocellulose paper by Western blotting. The immunoreacting protein bands were visualized after interacting with primary antibodies against cytochrome *c* and PARP and Bcl-2 as described before [9].

Wound healing motility assay

LNM35 and MDA-MB-231 cells were grown in six-well tissue culture dishes until they reach confluence. A scrape was made through the confluent monolayer with a plastic pipette tip of 1-mm diameter. Afterwards, dishes were washed twice and incubated at 37 °C in fresh RPMI containing 10% fetal calf serum in the presence or absence of the indicated concentrations of thymoquinone (1 and 10 μM). At the bottom side of each dish, two arbitrary places were marked where the width of the wound was measured with an inverted microscope (4×). Motility was expressed as the average ± SEM of the difference between the measurements at time zero and the 2–24 h time period.

Matrigel and Oris invasion assays

The invasiveness of the lung cancer cells LNM35 and breast cancer cells MDA-MB-231 treated with thymoquinone (1 and 10 μM) was tested using BD Matrigel Invasion Chamber (8-μm pore size; BD Biosciences, Le Pont de Claix, France). The PI3′-K inhibitor LY294002 (20 and 50 μM, respectively) was used as a positive inhibitor of cellular invasion. Cells (1×10^5 cells in 0.5 mL of media and the indicated concentration of thymoquinone) were seeded into the upper chambers of the system, and the bottom wells in the system were filled with RPMI supplemented with 10% fetal bovine serum as a chemo-attractant and then incubated at 37 °C for 24 h. Non-penetrating cells were removed from the upper surface of the filter with a cotton swab. Cells that have migrated through the matrigel were fixed with 4% formaldehyde, stained with DAPI, and counted in 20 random fields under a microscope. For quantification, the assay was performed in duplicates and repeated three times.

The Oris™ Cell Invasion Assay (AMS Biotechnology, Abingdon, UK) was used to investigate the impact of thymoquinone on MDA-MB-231-1833 cell invasion in vitro within a 3-dimensional extracellular matrix comprised of a basement membrane extract (BME) of the murine Engelbreth-Holm-Swarm tumor. Cells were seeded at 100 000 cells/well and allowed to attach overnight onto plates coated with BME solution. Once the cells formed a confluent monolayer, the silicone stoppers were removed and the cells treated with thymoquinone (1 and 10 μM) or the PI3′-K inhibitor LY294002 (20 μM). Following 48 h invasion, cells were labeled with Calcein AM (Invitrogen, CA, USA), and images were acquired, in the absence of the mask, by use of an Olympus fluorescence microscope.

Tumor growth and metastasis assay

Six-week-old athymic NMRI female nude mice (nu/nu, Elevage Janvier, France) were housed in filtered-air laminar flow cabinets and handled under aseptic conditions. Procedures involving animals and their care were conducted in conformity with Institutional guidelines that are in compliance with Faculty of

Medicine and Health Sciences, UAEU, National and International laws and policies (EEC Council Directive 86/609, OJ L 358, 1, December 12, 1987; and NIH Guide for Care and Use of Laboratory Animals, NIH Publication No. 85–23, 1985). Human Pulmonary LNM35 cells (1×10^6 cells) were injected subcutaneously into the lateral flank of the nude mice. One week after inoculation, when tumors had reached the volume of approximately 100 mm^3, animals (six in each group) were treated with thymoquinone (10 mg/kg, i.p.) or control (vehicle alone) 3 days per week (Sunday, Tuesday, and Thursday) for a total of 18 days. Tumor dimensions were measured with calipers every 3 days. Tumor volume (V) was calculated using the formula: $V = 0.4 \times a \times b^2$, with '$a$' being the length and '$b$' the width of the tumor. The animals were killed 18 days after treatment initiation, and the tumors and the axillary lymph nodes were excised, weighed, and fixed for immunohistochemical analysis.

Immunohistochemical determination of CD31/platelet-endothelial cell adhesion molecule 1 (PECAM-1) for microvessel density and cleaved caspase-3 for apoptotic cells

The effect of thymoquinone on angiogenesis was evaluated using CD31 immunostaining. The tumor tissues were quickly frozen in isopentane at −130 °C and stored at −70 °C until further processing. The frozen sections (8 μm) were fixed in acetone and incubated overnight with a CD31 antibody (1 : 400). Slides were then washed three times in PBS and incubated with secondary antibody (goat anti-rat 1 : 200) for one hour at room temperature. The sections were then stained with DAB and counterstained with hematoxylin. Vessel density was determined by counting the number of microvessels. The area occupied by CD31-positive microvessels and total tissue area per section were quantified and compared between treated and control mice. For individual tumors, the microvessel count was scored by averaging the counts from all fields. All analyses were performed in a blind fashion. The paraffin-embedded tissue sections (5 μm) were deparaffinized and then microwaved for 5 min for antigen retrieval. For the identification of apoptotic cells, cleaved caspase-3 staining was performed following the instructions of a commercially available Signal Stain Cleaved Caspase-3 (Asp175) IHC detection kit (Cellular SignalingTechnology, Beverly, MA, USA). Ten high-power fields (0.159 mm^2) per section of four to five tumors per treatment group were examined microscopically, and the average number of cells that stained positive for cleaved caspase-3 per treatment group was evaluated.

TarFisDock is a web-based tool for automating the procedure of searching for small molecule–protein interactions over a large repertoire of protein structures. It offers PDTD (potential drug target database), a target database containing 698 protein structures covering 15 therapeutic areas and a reverse ligand–protein docking program [10].

Potential Drug Target Database (PDTD) is a web-accessible protein database for *in silico* target identification. It currently contains >1100 protein entries with 3D structures presented in the Protein Data Bank. Data are extracted from the literatures and several online databases such as TTD, DrugBank, and Thomson Pharma. The database covers diverse information of >830 known or potential drug targets, including protein and active sites' structures in both PDB and mol2 formats, related diseases, biological functions as well as associated regulating (signaling) pathways. Each target is categorized by both nosology and biochemical function. In conjunction with TarFisDock, PDTD can be used to identify binding proteins for small molecules. The results can be downloaded in the form of mol2 file with the binding pose of the probe compound and a list of potential binding targets according to their ranking scores [11].

Statistical analysis

Results were expressed as means ± SEM. The difference between experimental and control values were assessed by ANOVA followed by Dunnett post hoc multiple comparison test. Tumor growth assays were analyzed using the unpaired Student's t-test. $P < 0.05$ indicates a significant difference.

RESULTS

Effect of thymoquinone on cell viability

As shown in *Figure 1*, exposure of LNM35, HepG2, HT29, MDA-MB-435, MDA-MB-231, and MCF-7 cells to increasing TQ concentrations (1–100 μM) for 24 h decreased cellular viability in a concentration-dependent manner. The IC_{50} concentrations (producing half-maximal inhibition) at 24 h were between 50 and 78 μM of TQ for all cells except for HepG2, and the IC_{50} was 34 μM of TQ. HepG2 cells seem to be the more sensitive cells to the cytotoxic effects of thymoquinone.

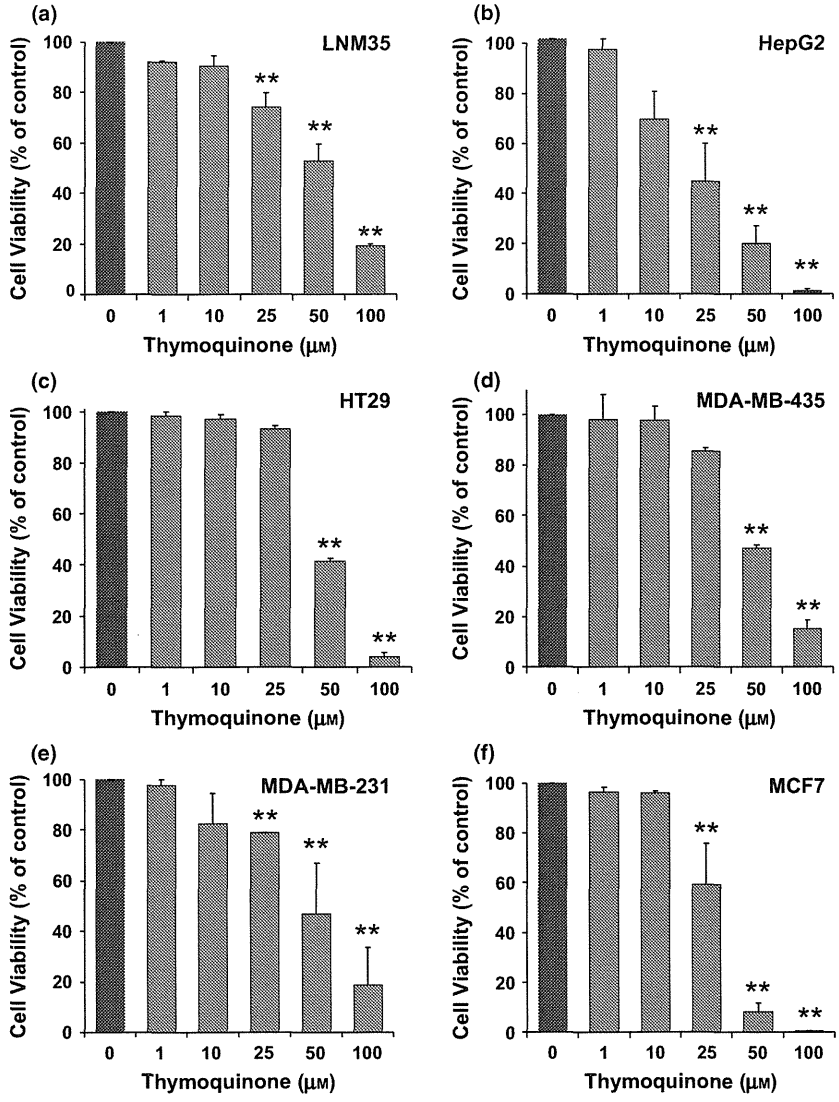

Figure 1 Inhibition of cellular viability by thymoquinone. Exponentially growing LNM35, HepG2, HT29, MDA-MB-435, MDA-MB-231, and MCF7 cells were treated for 24 h with vehicle (0.1% DMSO) and the indicated concentrations of thymoquinone. Viable cells were assayed as described in Materials and Methods. All experiments were repeated at least three times. *Columns*, mean; *bars*, SEM. **Significantly different at $P < 0.01$.

TQ treatment inhibits Akt phosphorylation and induces DNA damage in both MDA-MB-231 and LNM35 cancer cells

Phosphorylated Akt promotes cancer cell survival by inhibiting downstream apoptotic targets, such as proapoptotic Bcl-2 family member BAD and GSK-3 and increasing the survival targets such as Bcl-2. In this context, inhibition of the Akt pathway has been targeted as a promising strategy for cancer therapy. LNM35 and MDA-MB-231 cells were exposed to increasing concentrations of TQ for 30 min, 2, 6, and 24 h and total proteins were evaluated for phosphorylated Akt on serine 473. In both LNM35 and MDA-MB-231 cells, TQ induces a clear concentration and time-dependent inhibition of p-Akt (*Figure 2a*). These results indicate that the induction of apoptosis by TQ is at least in part associated with reduction in activated survival kinase Akt.

To check whether the induction of cell death by TQ is because of DNA damage, LNM35 as well as MDA-MB-231 cells were exposed to increasing concentrations of TQ for 30 min, 2, 6, and 24 h and total proteins were evaluated for γ-H_2aX expression. In both LNM35 and MDA-MB-231 cells, TQ induces a concentration and time-dependent increase in γ-H_2aX expression indicating that cell death induced by TQ was associated with induction of DNA damage (*Figure 2b*).

Cytochrome *c* release from mitochondria, caspase-3/7, and PARP activation

HepG2, the more sensitive cells to the cytotoxic effect of TQ, were used to determine whether the thymoquinone

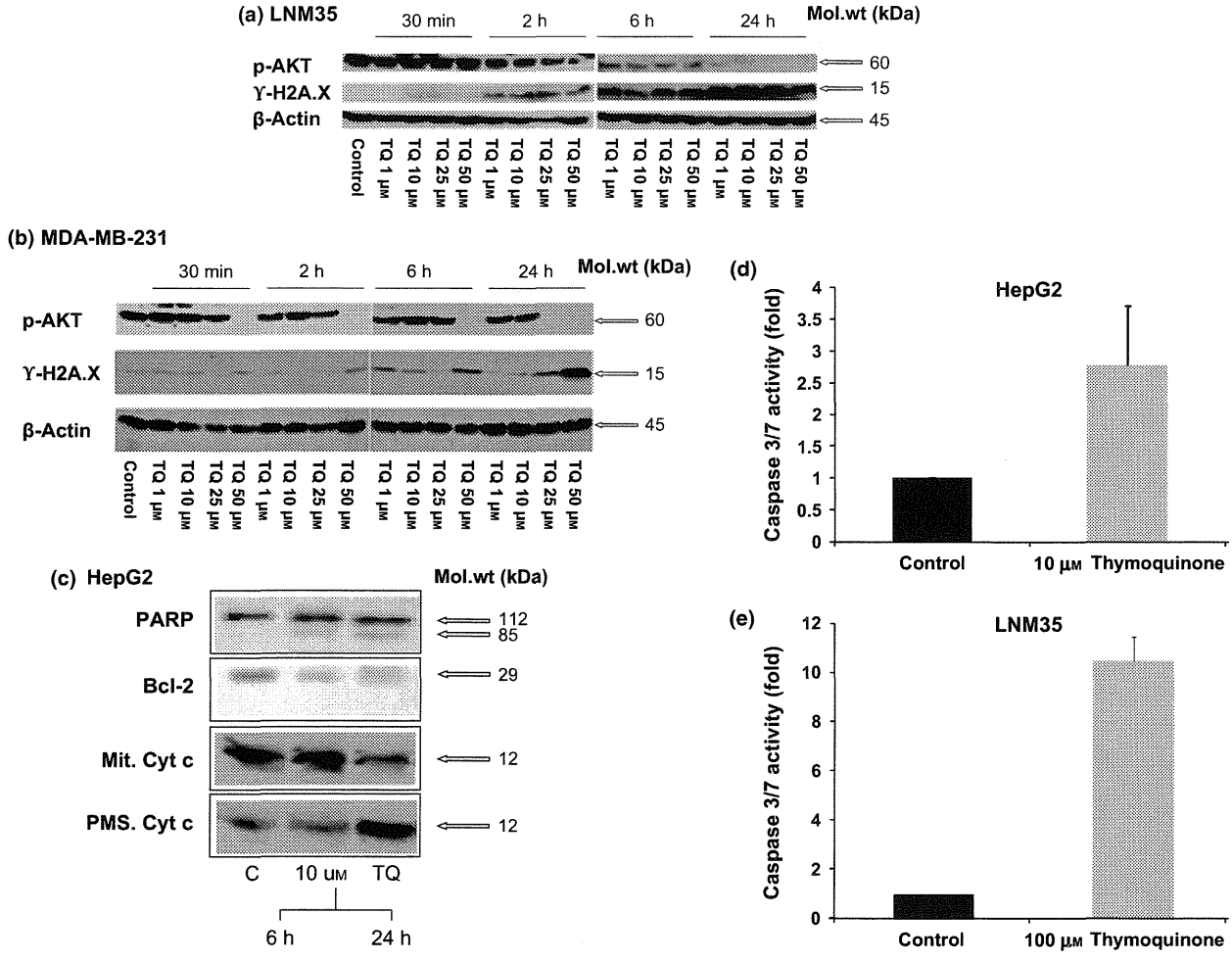

Figure 2 Phosphorylation of Akt and H_2aX, cytochrome *c* release, induction of caspase-mediated apoptosis PARP activation by thymoquinone. Indicated cells were exposed to increasing concentrations of TQ, and total proteins were collected after 30 min, 2, 6, and 24 h, and the phosphorylation of Akt and H_2aX protein was assessed by immunoblot in (a) LNM35 and (b) MDA-MB-231 cells. (c) Human hepatoma cancer cells HepG2 were treated with vehicle (0.1% DMSO) or 10 µM of thymoquinone for 6 h. c, upper panel) PARP cleavage in HepG2 cells treated with thymoquinone 10 µM and incubated for incubated for 6 and 24 h. Cleavage of PARP was detected by Western blotting; 112- and 85-kDa protein bands indicated native and cleaved PARP, respectively. c, lower panel) Cytochrome *c* expression in the mitochondria and postmitochondrial supernatants (PMS). (d) Induction of caspase-3/7 activity by thymoquinone in HepG2 cells and (e) in LNM35 cells. Caspase-3/7 activity was determined using the Caspase-Glo 3/7 assay and was normalized to the number of viable cells per well and expressed as fold induction compared with the control group.

effect was because of apoptosis. Western blot analysis of the HepG2 cells revealed that 6 and 24 h treatment with 10 µM thymoquinone caused an increase in the release of cytochrome *c* from the mitochondria as compared to the control cells (*Figure 2c*). In a sequential manner, once the cytochrome *c* released into cytosol, it recruits and activates caspases that are the executioners of apoptosis. To determine whether cells were undergoing apoptosis, the activity of the main effector caspases, caspases-3 and -7, was analyzed using the Caspase-Glo 3/7 assay 6 h after treatment with TQ (10 µM). The relative caspase activity was normalized to the number of cells per well and compared to the control cells. A significant 2.7 fold increase in caspase-3 and -7 activities was observed in HepG2 cells (*Figure 2d*). To confirm that LNM35 cells also were undergoing apoptosis after exposure to thymoquinone, caspase-3/7 was measured 24 h after treatment with TQ (100 µM). A 10 folds increase in caspase-3/7 activity was observed in LNM35 cells after treatment with TQ

100 μM (*Figure 2e*). Poly-(ADP-ribose) polymerase-1 (PARP-1) is a nuclear enzyme involved in DNA repair and stability downstream of caspase-3/7 activation. Cleavage of PARP-1 is used as a hallmark of caspase-3/7 activation and apoptosis. PARP-1 cleavage during apoptosis impairs the DNA repair capacity of the cell. Intact PARP (112 kDa) was seen in DMSO-treated HepG2 cells. However, after 6 and 24 h treatment of HepG2 cells with 10 μM of thymoquinone, PARP was cleaved into an 85 kDa fragment as a result of caspase-3/7 activation and which is consistent with cell death that results from apoptosis (*Figure 2c*). We also demonstrated a reduced expression of BcL-2 in HepG2 cells after TQ treatment (*Figure 2c*).

Impact of thymoquinone on cancer cell motility and invasion

Using a classic in vitro wound healing model, we assessed whether thymoquinone was able to inhibit epithelial cell motility. Thymoquinone was found to be ineffective in reducing cellular motility in the LNM35 cells (*Figure 3a*); similarly, the dose- and time-dependant inhibition observed in the MDA-MB-231 was also not statistically significant even after 6 h incubation with TQ 10 μM (*Figure 3b*).

However, TQ was able to significantly reduce the invasiveness of both LNM35 and MDA-MB-231 cells in matrigel invasion assay (*Figure 4a,b*). The inhibition of matrigel invasion seen following exposure of cells to low concentrations of TQ (0.1, 1, and 10 μM) occurred

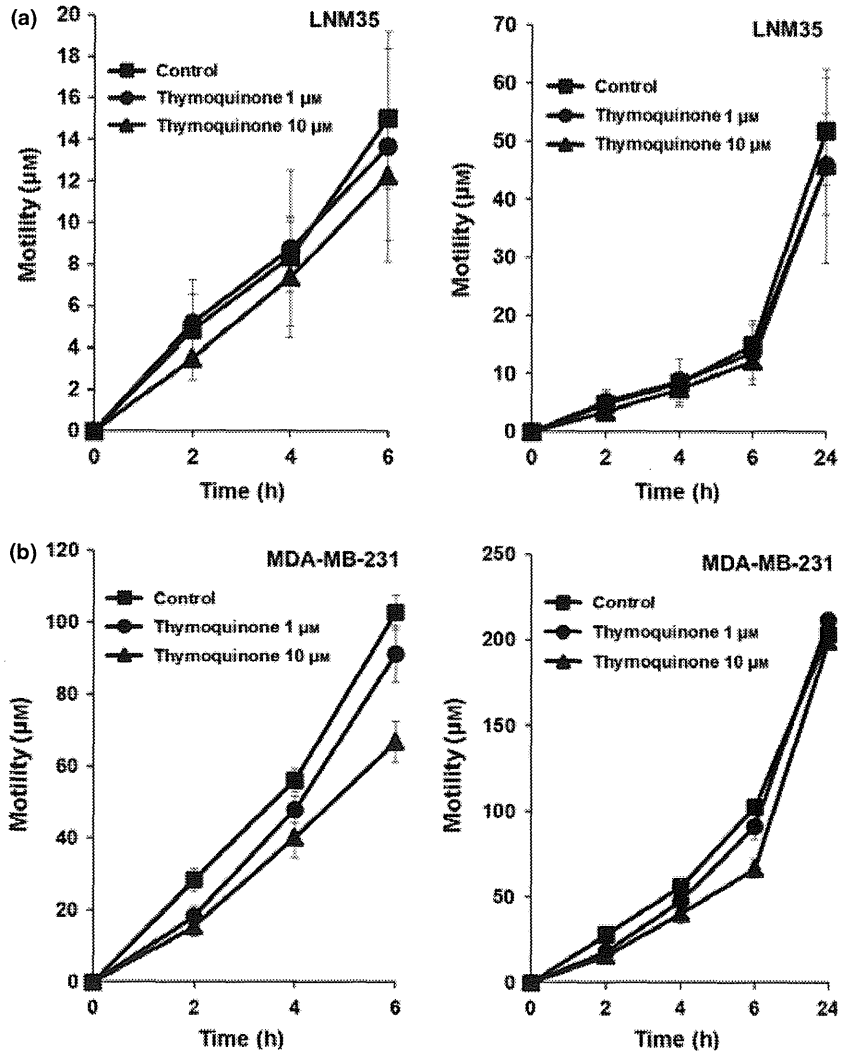

Figure 3 Dose–response effect of thymoquinone on cellular motility. Wounds were introduced in confluent monolayers LNM35 (a) and MDA-MB-231 (b) cells in the presence or absence (control) of thymoquinone (1 and 10 μM). The mean distance that cells travelled from the edge of the scraped area for 2, 4, 6, and 24 h at 37 °C was measured in a blinded fashion, using an inverted microscope (4× magnifications). Data are means ± SEM of two independent experiments.

without reduction in cell viability (*Figure 1a,e*). Next, we investigated the impact of non-toxic concentration of 1 μM of TQ (*Figure 4c*) on the invasiveness of the highly invasive breast cancer cells MDA-MB231-1833 using Oris invasion assay. Again, TQ reduced the invasiveness of these cells at the non-toxic concentration of 1 μM (*Figure 4d*). We conclude that TQ significantly reduced the invasive potential of lung cancer (LNM35) and breast cancer (MDA-MB231 and MDA-MB231-1833) cells.

In vivo impact of thymoquinone on tumor growth

The anticancer activity of TQ was investigated in athymic mice inoculated with the highly tumorigenic LNM35 human lung cells as xenografts. TQ reduced the growth of LNM35 human tumor xenografts by 39% at day 18 (*Figure 5a*). There was no sign of toxicity because of thymoquinone administration and no significant difference in body weight between the thymoquinone-treated animals and the control group (data not shown). The effect of TQ on tumor angiogenesis was assessed by CD31-immunostaining of LNM35 tumor tissue xenografts. CD31 is specifically expressed on the surface of endothelial cells and is weakly expressed on lymphoid cells and platelets. Immunohistochemical analysis indicated that when the CD31-positive areas or number of microvessels was normalized to tumor area, TQ vs. control did not cause vascular regression in the tumors. LNM35 tumor growth inhibition was associated with a significant increase in caspase-3 activity similar to the in vitro results indicating that the tumor growth inhibition induced by TQ is mainly due to the induction of apoptosis (*Figure 5b*). Next, we assessed the metastatic behavior of the human pulmonary cell

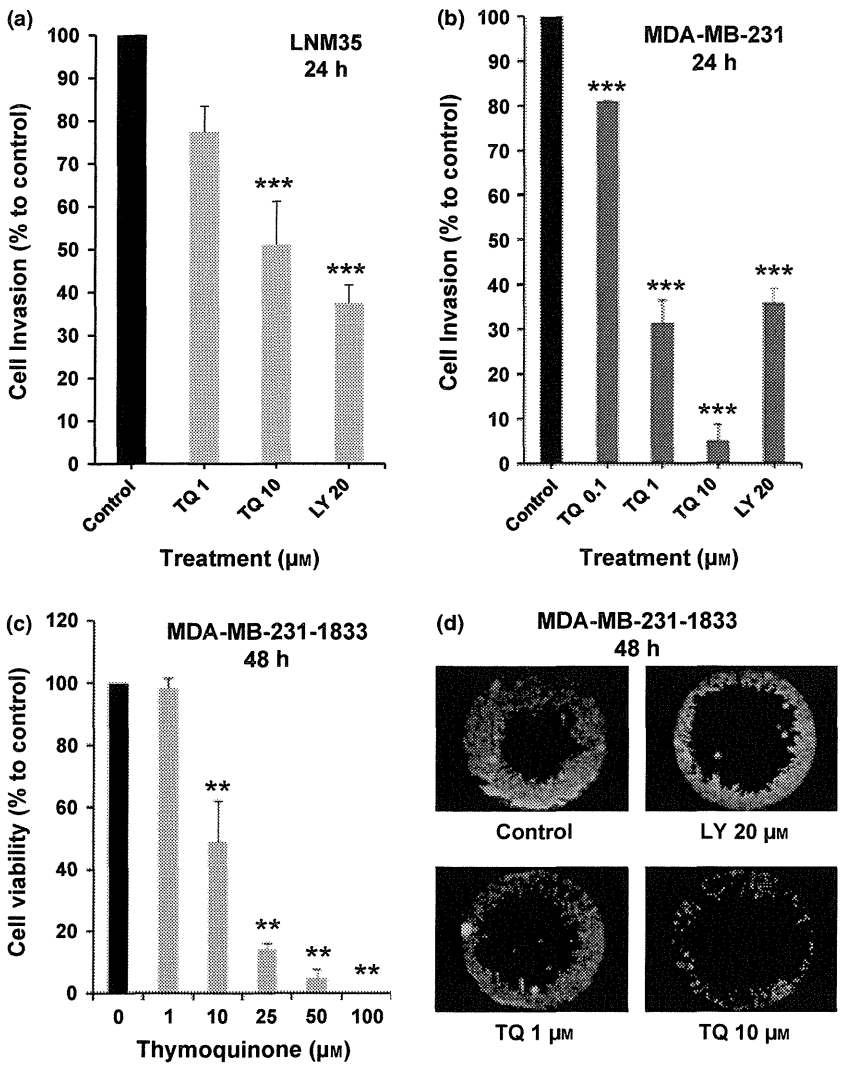

Figure 4 Dose effect of thymoquinone on matrigel and Oris cell invasion assay. (a) LNM35; (b) MDA-MB-231 cells were incubated for 24 h in the presence or absence of thymoquinone (0.1–10 μM). Cells that invaded into matrigel were scored as described in Materials and Methods. *Columns*, mean; bars, SEM. (c) MDA-MB-213-1833 cells were treated with vehicle for 48 h (0.1% DMSO) and the indicated concentrations of TQ. Viable cells were assayed as described in Materials and Methods. (d) MDA-MB-213-1833 cells were incubated for 48 h in the presence or absence of thymoquinone (1 and 10 μM), LY (20 μM) onto an Oris cell invasion assay plate. Cell invasion images were acquired by inverted microscope as described in Materials and Methods. Experiments were repeated at least three times. Columns, mean; bars, SEM. **Significantly different at $P < 0.01$, ***Significantly different at $P < 0.001$.

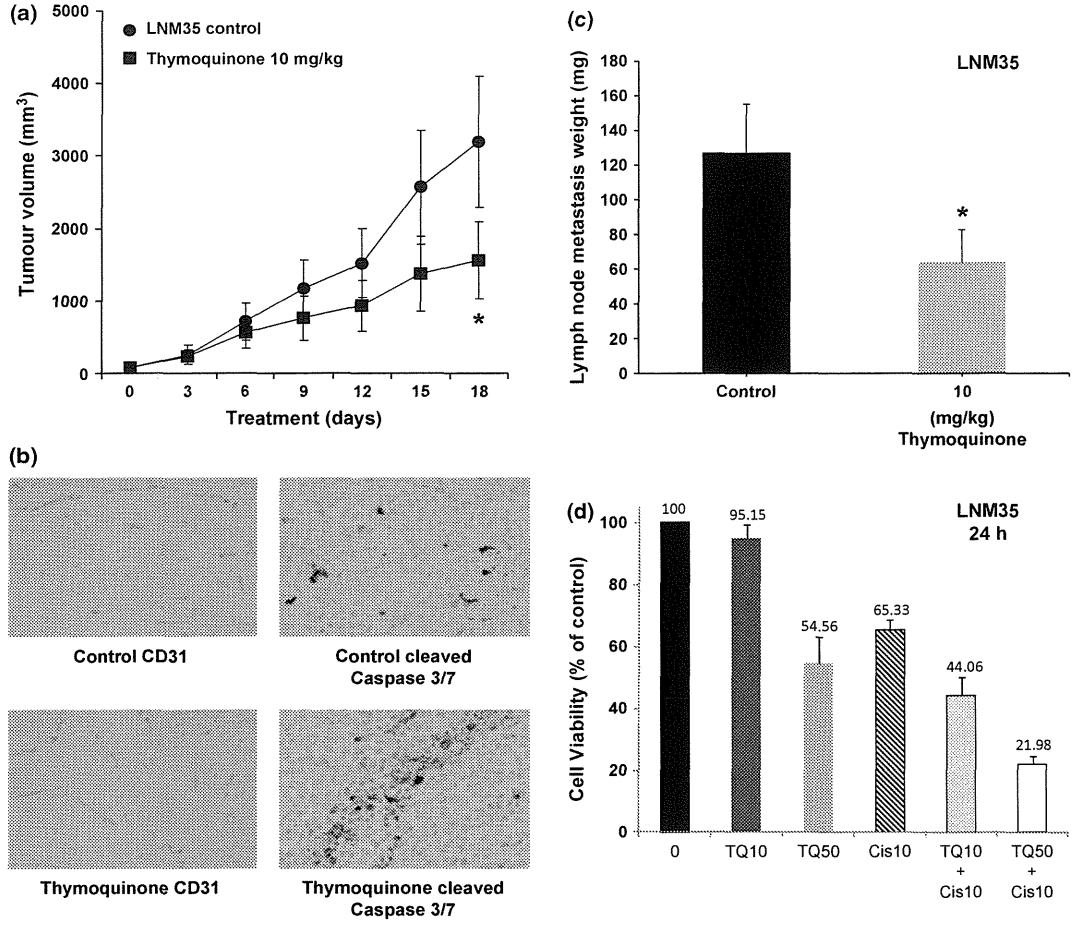

Figure 5 Impact of thymoquinone on the tumor volume, angiogenesis, cancer cell death, and metastasis of established human lung cancer xenografts. (a) Nude mice were xenografted S.C. with human lung LNM35 cancer cells (10^6 cells per animal) and treated with thymoquinone (10 mg/kg, i.p) or control (carrier solution alone) 3 days per week (Sunday, Tuesday, and Thursday) for a total of 18 days. Data points represent the mean ± SEM of 6 to 7 mice per group. Statistically significant differences are indicated in (a) for tumor volume (*$P < 0.05$ vs. control). (b) Immunohistochemical staining for CD31 (right panel) and cleaved caspase-3/7 (left panel) in LNM35 human lung cancer growing in nude mice treated with saline (control) and thymoquinone. (c) Lymph nodes metastasis weight of established human lung cancer xenografts treated with TQ 10 mg/kg for 18 days. *Columns*, mean; *bars*, SEM. (d) LNM35 cells were incubated in the presence or absence of thymoquinone (10 and 50 μM), cisplatin (10 μM) or with combined thymoquinone and cisplatin treatment for 24 h. Cell viability was measured as described in Materials and Methods. All experiments were repeated at least three times. *Columns*, mean; *bars*, SEM.

line LNM35 by examining axillary lymph nodes. In the control-treated group, the mean lymph nodes weight was 127 ± 28.1 mg compared with 63.5 ± 19.2 mg in the groups treated with TQ 10 mg/kg/day for 18 days (*Figure 5c*).

Thymoquinone synergizes with cisplatin to inhibit cellular viability

Our *in vivo* data encouraged us to investigate the possible contribution of TQ to enhance the cytotoxicity of cisplatin in the human NSCLC lung cell line LNM35 in vitro. Interestingly, low to moderate concentrations of TQ (10 and 50 μM) revealed a synergistic inhibition of LNM35 cell viability in vitro in combination with cisplatin (10 μM) (*Figure 5d*).

An attempt to identify a target for thymoquinone

In an attempt to suggest possible targets for thymoquinone, we carried out a short chemo-informatics study combining a reverse docking procedure and a ligand-based similarity approach. In the former approach, we used the TarFisDock web server to reverse dock TQ on

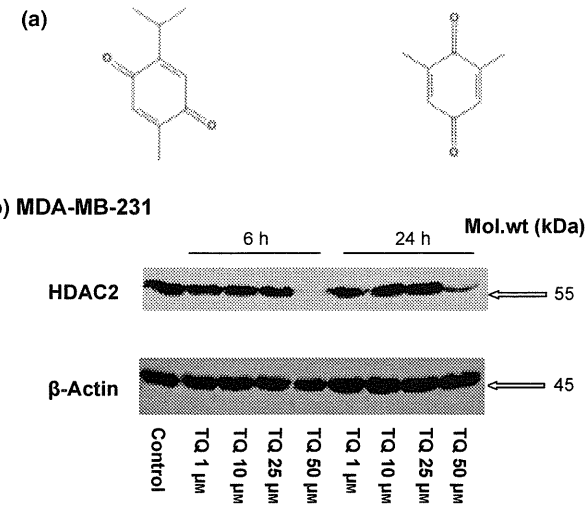

Figure 6 (a) 2D sketches of THQ (Left) and 2, 6-dimethyl-1, 4-benzoquinone (Right) that have a 0.84 pairwise Tanimoto coefficient. (b) MDA-MB-231 cells were exposed to increasing concentrations of TQ, and total proteins were collected after 6 and 24 h, and the expression of HDAC2 protein was assessed by immunoblot.

1207 different protein structures. This corresponds to 841 different protein targets spanning through a vast array of protein types and associated diseases. Among the results, we found several potential targets for TQ that are known to be involved cancer, such as Carboxypeptidase A (Pancreatic Cancer), Thymidine Kinase (Bladder Cancer), HDAC-2 (Colon Cancer), and Nuclear Vitamin D Receptor (Colorectal and Prostate Cancer). In the ligand-based similarity approach, we used the PubChem server to detect similar compounds to TQ (Tanimoto index above 0.8), and we analyzed the PubChem BioAssay results available for those compounds. Interestingly, only one compound, 2, 6-dimethyl-1, 4-benzoquinone (*Figure 6a*) has been identified as active within a PubChem Bioassay whose protein target was clearly identified (Pubchem Bioassay AID388). The associated target is the human 15-hydroxyprostaglandin dehydrogenase (HPGD). In this context, we demonstrated that TQ treatment for 6 and 24 h resulted in a significant inhibition of HDAC2 proteins (*Figure 6b*).

DISCUSSION

Nigella sativa popularly known as black seed has been used in traditional medicine for the treatment of a variety of illnesses, including bronchial asthma, headache, dysentery, infections, obesity, back pain, hypertension, gastrointestinal problems, and eczema [4]. Several bioactive components of black seed have been identified, including thymoquinone, thymol, thymohydroquinone, and dithymoquinone. Among them thymoquinone (TQ) has been reported to exhibit antioxidant, anti-inflammatory, and chemopreventive effects [3,4,12].

Results presented in this study demonstrate that thymoquinone induces cell death of several human cancer cell lines derived from lung, liver, colon, melanoma, and breast cancer. These results are in line with several other studies that have demonstrated that thymoquinone induced apoptosis in cancer cell lines including myeloblastic leukemia, pancreatic, ovarian, breast and colorectal adenocarcinoma [4,5,13–15].

Previous studies reported that thymoquinone induced apoptosis in tumor cells by suppressing COX-2, survivin, Bcl family proteins, STAT3 phosphorylation, NF-κB, Akt activation, extracellular signal-regulated kinase (ERK), and inhibition of telomerase activity leading to telomere shortening [6,12,16–19]. A recent study proposed a new mechanism for the antineoplastic effect of TQ. The authors demonstrate that treatment with TQ induced ROS generation, which increased JNK and ERK in an attempt to bypass the stress injury. However, ERK and JNK fail to confer a survival role, and the cells undergo apoptosis [20].

It has been reported that Akt activation may allow cells to evade the deleterious consequences of DNA damage, and consequently, the inhibition of Akt phosphorylation will markedly enhance DNA damage [21]. The γ-H_2aX, phosphorylated histone H_2AX, formation is an early chromatin modification event that follows initiation of DNA fragmentation during apoptosis before DNA repair. We present strong evidence that the antineoplastic effect of TQ is at least in part, associated with induction of the DNA damage protein H_2aX in both breast and lung cancer cells. These results are in line with similar finding in colon cancer cells [22]. In this context, we provided mechanistic evidences that TQ-induced cell death is mediated, at least in part, by inhibition of the phosphorylation of the survival serine threonine kinase Akt leading to phosphorylation of γ-H_2aX.

Induction of apoptosis is a key factor in the response of tumors to chemotherapy. Cells can respond to DNA damage either by undergoing cell cycle arrest, to facilitate DNA repair, or by undergoing cell suicide. Apoptosis is a major form of cell death involving the

mitochondria (intrinsic pathway) or death receptors (extrinsic pathway). The intrinsic pathway involves the release of cytochrome *c* from the intermembrane space of the mitochondria leading to the activation of downstream caspase-3/7 that leads to the cleavage of PARP and the death response [23]. In this context, we determined the nature of cell death induced by TQ in our cancer cells, which engages the mitochondrial pathway, allowing the release of cytochrome *c*. Our results also show that TQ activates the apoptotic pathway, as evidenced by the activation of caspase-3/7, the main effector of apoptosis. These results are in line with previous studies indicating that caspase-3 activation-mediated the TQ-induced apoptosis in myeloblastic leukemia HL-60 cells and human laryngeal carcinoma cells HEp-2 [15,24]. Caspase-3 recognizes the DEVD motif within the amino-terminal domain of PARP-1 and cleaves this nuclear enzyme between amino acids 214 and 215 [25]. In this study, a p85 protein band representing the caspase-3 cleaved PARP-1 was generated in HepG2 cells after exposure to TQ.

In this study, we reported that treatment with non-toxic concentrations of thymoquinone (0.01, 0.1 and 1 μM) inhibits the invasiveness of human lung cancer cells LNM35 and human mammary adenocarcinoma cells (MDA-MB-231 and MDA-MB-213-1833). This ability of low concentration of TQ (0.1–10 μM) to reduce the invasiveness of breast cancer cells was also reported recently [26]. In line with our results, recent studies indicated that thymoquinone exhibits significant inhibitory effect on HGF-induced HepG2 hepatoma cell motility and invasion; VEGF-induced PC3 prostate cancer cell motility, on human umbilical vein endothelial cell (HUVEC) motility and invasion and also glioblastoma cells associated with FAK, MMP-2, and MMP-9 downregulation [17,27]. Similarly, high concentration of TQ (20–80 μM) significantly inhibits mouse C26 colon cancer cell invasion, pancreatic cancer cell invasion and metastasis as well as human NCI-H460 lung cancer cell invasion [28]. Taken together, these results confirm that the impact of thymoquinone on cancer cell motility and invasion is not tissue specific and suggests a potent antimetastatic effect of TQ. In this context, we demonstrated that TQ significantly reduces metastasis *in vivo*.

The chemotherapeutic agents currently in use for lung cancer are still unsatisfactory because of associated co-lateral toxicity and drug-induced resistance that encouraged us to investigate *in vivo* the anticancer activity of thymoquinone in athymic mice xenografted with the LNM35 human lung cells. Previous reports have demonstrated that the LD50 of TQ after intraperitonial injection to mice were 104.7 mg/kg [29]. A phase I study conducted by Al-Amri and Bamosa had reported no significant systemic toxicities in adult patients with solid tumors or hematological malignancies who were treated with thymoquinone [30]. It was also found that the human body could tolerate a dose of thymoquinone up to 2600 mg/day [3]. We demonstrated that intraperitonial administration of thymoquinone (10 mg/kg, 10 times less that the LD50 dose) for 18 days slows down LNM35 lung tumor growth by 39% without manifest side effects. It has also been demonstrated previously that thymoquinone (10 mg/kg) does not induce mortality or any pathological abnormalities in the lung, heart, or kidneys [31]. Our findings are in agreement with other studies showing that TQ (5–20 mg/kg/day) inhibits growth of HCT116 colon cancer and PC3 prostate cancer xenografts [17,28,32]. To determine the mechanism by which thymoquinone inhibits tumor growth, we investigated the impact of this compound on tumor cell survival and angiogenesis using cleaved caspases-3 and CD31 antibodies, respectively. We found that the tumor growth inhibition was associated with significant increase in apoptosis as reported in colon cancer xenografts treated with TQ [28], in contrast with previous report related to potential antiangiogenic effect of TQ [17]. In this study, the antineoplastic effect of TQ does not appear to be due to the inhibition of angiogenesis. At least at the dose of TQ used, no significant difference in neo-angiogenesis was observed between TQ and control LNM35 tumor xenografts.

Clinical trials revealed that single agent treatments rarely result in clinical benefits to cancer patients, suggesting that combination therapy is necessary for effective treatment for majority of cancers. Emerging evidence demonstrates that thymoquinone in combination with gemcitabine and/or oxaliplatin is superior as an antitumor agent compared with either agent alone [16]. It has been reported that TQ potentiates the antitumor activity of cisplatin and improves its therapeutic index in Ehrlich ascites carcinoma and also reduces the toxic effects of various anticancer drugs including cisplatin and doxorubicin [33,34]. Cisplatin is widely used in the treatment of lung, bladder, ovarian, and cervical cancer [35]. The first-line chemotherapeutic protocol in lung cancer is cisplatin in combination with paclitaxel, docetaxel, vinorelbine, gemcitabine, or irinotecan [36]. We examined the

possibility to enhance lung cancer cell death of cisplatin by combination with TQ. Our in vitro data indicate that combination of TQ and cisplatin caused greater inhibition of LNM35 lung cancer cell viability than each drug given alone. Recent study also showed a synergism between TQ and cisplatin in inhibition of the NCI-H460 lung cell proliferation as well as tumor growth [31]. Building on aforementioned results, which strongly support better killing of lung cancer cells when exposed to both cisplatin and thymoquinone, we will evaluate in future plan the therapeutic advantage of combination of cisplatin and thymoquinone in nude mice bearing LNM35 xenografts.

Interestingly, the identification of HDAC-2 among the potential protein targets and the demonstration in this study that TQ treatment leads to a decrease in HDAC2 protein level corroborates the recent findings suggesting that TQ inhibits histone deacetylase (HDAC) activity and induces histone hyperacetylation [37]. On the other hand, the human 15-hydroxyprostaglandin dehydrogenase (HPGD) is a target that has been recently associated with higher risk for colorectal cancer [38], and it is now known that TQ can inhibit tumor growth in murine colon cancer models [28]. Taken together, these preliminary results suggest several potential targets (mainly HDAC proteins and HPGD) and seem to corroborate the previously published studies on the effect of TQ cancer progression.

In conclusion, we provide evidence that TQ induces cancer cell death at least in part via inhibition of Akt phosphorylation leading DNA damage and activation of the mitochondrial-signaling proapoptotic pathway. Furthermore, TQ is also able to reduce the invasiveness of cancer cells and to sensitize LNM35 cancer cells to the cytotoxic effects of the DNA-damaging agent cisplatin. We also report an anticancer effect of TQ in a highly aggressive human lung cancer xenograft in nude mice. Recent study presented preliminary evidence for novel synthetic TQ analogs with biological activity that is better than the parental TQ without systemic toxicity [39]. In view of the available experimental findings, we contend that thymoquinone and /or its analogues may have a strong clinical potential as an anticancer drug either alone or in combination with some chemotherapeutic agents such as cisplatin.

ACKNOWLEDGEMENTS

This work was financially supported by the Research Affairs at the UAE University under a contract no. 02-04-8-11/07 and by Terry Fox Fund for Cancer Research to samir Attoub and haider Raza. The authors wish to thank Ms. Anne John and Ms. Manjusha Sudhadevi, Dept. of Pathology, Ms. Annie John, Dept. of Biochemistry FMHS for their excellent technical help. We thank Prof. Joan Massague from Howard Hughes Medical Institute for providing the MDA-MB-231 and MDA-MB-231-1833 cells and Dr. Mien-Chie Hung from University of Texas MD Anderson Cancer Center for providing the MDA-MB-435 cells.

REFERENCES

1 Parkin D.M., Bray F., Ferlay J., Pisani P. Global cancer statistics, 2002. CA Cancer J. Clin. (2005) **55** 74–108.
2 Gali-Muhtasib H., Roessner A., Schneider-Stock R. Thymoquinone: a promising anti-cancer drug from natural sources. Int. J. Biochem. Cell Biol. (2006) **38** 1249–1253.
3 Woo C.C., Kumar A.P., Sethi G., Tan K.H. Thymoquinone: potential cure for inflammatory disorders and cancer. Biochem. Pharmacol. (2011) **83** 443–451.
4 Gali-Muhtasib H., Diab-Assaf M., Boltze C., et al. Thymoquinone extracted from black seed triggers apoptotic cell death in human colorectal cancer cells via a p53-dependent mechanism. Int. J. Oncol. (2004) **25** 857–866.
5 Rooney S., Ryan M.F. Effects of alpha-hederin and thymoquinone, constituents of *Nigella sativa*, on human cancer cell lines. Anticancer Res. (2005) **25** 2199–2204.
6 Gurung R.L., Lim S.N., Khaw A.K., Soon J.F., Shenoy K., Mohamed Ali S. et al. Thymoquinone induces telomere shortening, DNA damage and apoptosis in human glioblastoma cells. PLoS ONE (2010) **5** e12124.
7 Kozaki K., Miyaishi O., Tsukamoto T., Tatematsu Y., Hida T., Takahashi T. Establishment and characterization of a human lung cancer cell line NCI-H460-LNM35 with consistent lymphogenous metastasis via both subcutaneous and orthotopic propagation. Cancer Res. (2000) **60** 2535–2540.
8 Raza H., Prabu S.K., Robin M.A., Avadhani N.G. Elevated mitochondrial cytochrome P450 2E1 and glutathione S-transferase A4-4 in streptozotocin-induced diabetic rats: tissue-specific variations and roles in oxidative stress. Diabetes (2004) **53** 185–194.
9 Raza H., John A. 4-hydroxynonenal induces mitochondrial oxidative stress, apoptosis and expression of glutathione S-transferase A4-4 and cytochrome P450 2E1 in PC12 cells. Toxicol. Appl. Pharmacol. (2006) **216** 309–318.
10 Li H., Gao Z., Kang L., Zhang H., Yang K., Yu K. et al. TarFisDock: a web server for identifying drug targets with docking approach. Nucleic Acids Res. (2006) **34** W219–W224.
11 Gao Z., Li H., Zhang H., Liu X., Kang L., Luo X. et al. PDTD: a web-accessible protein database for drug target identification. BMC Bioinformatics (2008) **9** 104.

12 Sethi G., Ahn K.S., Aggarwal B.B. Targeting nuclear factor-kappa B activation pathway by thymoquinone: role in suppression of antiapoptotic gene products and enhancement of apoptosis. Mol. Cancer Res. (2008) **6** 1059–1070.
13 Worthen D.R., Ghosheh O.A., Crooks P.A. The in vitro anti-tumor activity of some crude and purified components of blackseed, *Nigella sativa* L. Anticancer Res. (1998) **18** 1527–1532.
14 Shoieb A.M., Elgayyar M., Dudrick P.S., Bell J.L., Tithof P.K. In vitro inhibition of growth and induction of apoptosis in cancer cell lines by thymoquinone. Int. J. Oncol. (2003) **22** 107–113.
15 El-Mahdy M.A., Zhu Q., Wang Q.E., Wani G., Wani A.A. Thymoquinone induces apoptosis through activation of caspase-8 and mitochondrial events in p53-null myeloblastic leukemia HL-60 cells. Int. J. Cancer (2005) **117** 409–417.
16 Banerjee S., Kaseb A.O., Wang Z., Kong D., Mohammad M., Padhye S. et al. Antitumor activity of gemcitabine and oxaliplatin is augmented by thymoquinone in pancreatic cancer. Cancer Res. (2009) **69** 5575–5583.
17 Yi T., Cho S.G., Yi Z., Pang X., Rodriguez M., Wang Y. et al. Thymoquinone inhibits tumor angiogenesis and tumor growth through suppressing AKT and extracellular signal-regulated kinase signaling pathways. Mol. Cancer Ther. (2008) **7** 1789–1796.
18 Li F., Rajendran P., Sethi G. Thymoquinone inhibits proliferation, induces apoptosis and chemosensitizes human multiple myeloma cells through suppression of signal transducer and activator of transcription 3 activation pathway. Br. J. Pharmacol. (2010) **161** 541–554.
19 Arafa e.-S., Zhu Q., Shah Z.I., Wani G., Barakat B.M., Racoma I. et al. Thymoquinone up-regulates PTEN expression and induces apoptosis in doxorubicin-resistant human breast cancer cells. Mutat. Res. (2011) **706** 28–35.
20 El-Najjar N., Chatila M., Moukadem H., Vuorela H., Ocker M., Gandesiri M. et al. Reactive oxygen species mediate thymoquinone-induced apoptosis and activate ERK and JNK signaling. Apoptosis (2010) **15** 183–195.
21 Xu N., Hegarat N., Black E.J., Scott M.T., Hochegger H., Gillespie D.A. Akt/PKB suppresses DNA damage processing and checkpoint activation in late G2. J. Cell Biol. (2010) **190** 297–305.
22 Gali-Muhtasib H., Kuester D., Mawrin C., Bajbouj K., Diestel A., Ocker M. et al. Thymoquinone triggers inactivation of the stress response pathway sensor CHEK1 and contributes to apoptosis in colorectal cancer cells. Cancer Res. (2008) **68** 5609–5618.
23 Fesik S.W. Promoting apoptosis as a strategy for cancer drug discovery. Nat. Rev. Cancer (2005) **5** 876–885.
24 Rooney S., Ryan M.F. Modes of action of alpha-hederin and thymoquinone, active constituents of *Nigella sativa*, against HEp-2 cancer cells. Anticancer Res. (2005) **25** 4255–4259.
25 Wesierska-Gadek J., Gueorguieva M., Wojciechowski J., Tudzarova-Trajkovska S. In vivo activated caspase-3 cleaves PARP-1 in rat liver after administration of the hepatocarcinogen N-nitrosomorpholine (NNM) generating the 85 kDa fragment. J. Cell. Biochem. (2004) **93** 774–787.
26 Woo C.C., Loo S.Y., Gee V., Yap C.W., Sethi G., Kumar A.P. et al. Anticancer activity of thymoquinone in breast cancer cells: possible involvement of PPAR-γ pathway. Biochem. Pharmacol. (2011) **82** 464–475.
27 Kolli-Bouhafs K., Boukhari A., Abusnina A., Velot E., Gies J. P., Lugnier C. et al. Thymoquinone reduces migration and invasion of human glioblastoma cells associated with FAK, MMP-2 and MMP-9 down-regulation. Invest. New Drugs (2011).
28 Gali-Muhtasib H., Ocker M., Kuester D., Krueger S., El-Hajj Z., Diestel A. et al. Thymoquinone reduces mouse colon tumor cell invasion and inhibits tumor growth in murine colon cancer models. J. Cell Mol. Med. (2008) **12** 330–342.
29 Al-Ali A., Alkhawajah A.A., Randhawa M.A., Shaikh N.A. Oral and intraperitoneal LD50 of thymoquinone, an active principle of *Nigella sativa*, in mice and rats. J. Ayub Med. Coll. Abbottabad (2008) **20** 25–27.
30 Al-Amri A.M., Bamosa A.O. Phase I safety and clinical activity study of thymoquinone in patients with advanced refractory malignant disease. Shiraz E-Med. J. (2009) **10** 107–111.
31 Jafri S.H., Glass J., Shi R., Zhang S., Prince M., Kleiner-Hancock H. Thymoquinone and cisplatin as a therapeutic combination in lung cancer: in vitro and in vivo. J. Exp. Clin. Cancer Res. (2010) **29** 87.
32 Kaseb A.O., Chinnakannu K., Chen D., Sivanandam A., Tejwani S., Menon M. et al. Androgen receptor and E2F-1 targeted thymoquinone therapy for hormone-refractory prostate cancer. Cancer Res. (2007) **67** 7782–7788.
33 Badary O.A., Nagi M.N., al-Shabanah O.A., al-Sawaf H.A., al-Sohaibani M.O., al-Bekairi A.M. Thymoquinone ameliorates the nephrotoxicity induced by cisplatin in rodents and potentiates its antitumor activity. Can. J. Physiol. Pharmacol. (1997) **75** 1356–1361.
34 Nagi M.N., Mansour M.A. Protective effect of thymoquinone against doxorubicin-induced cardiotoxicity in rats: a possible mechanism of protection. Pharmacol. Res. (2000) **41** 283–289.
35 Ferraldeschi R., Baka S., Jyoti B., Faivre-Finn C., Thatcher N., Lorigan P. Modern management of small-cell lung cancer. Drugs (2007) **67** 2135–2152.
36 Lally B.E., Urbanic J.J., Blackstock A.W., Miller A.A., Perry M. C. Small cell lung cancer: have we made any progress over the last 25 years? Oncologist (2007) **12** 1096–1104.
37 Chehl N., Chipitsyna G., Gong Q., Yeo C.J., Arafat H.A. Anti-inflammatory effects of the *Nigella sativa* seed extract, thymoquinone, in pancreatic cancer cells. HPB (Oxford) (2009) **11** 373–381.
38 Hoeft B., Linseisen J., Beckmann L., Müller-Decker K., Canzian F., Hüsing A. et al. Polymorphisms in fatty-acid-metabolism-related genes are associated with colorectal cancer risk. Carcinogenesis (2010) **31** 466–472.
39 Banerjee S., Azmi A.S., Padhye S., Singh M.W., Baruah J.B., Philip P.A. et al. Structure-activity studies on therapeutic potential of Thymoquinone analogs in pancreatic cancer. Pharm. Res. (2010) **27** 1146–1158.

PLOS | ONE

Frondoside A Suppressive Effects on Lung Cancer Survival, Tumor Growth, Angiogenesis, Invasion, and Metastasis

Samir Attoub[1]*, Kholoud Arafat[1], An Gélaude[2], Mahmood Ahmed Al Sultan[1], Marc Bracke[2], Peter Collin[3], Takashi Takahashi[4], Thomas E. Adrian[5], Olivier De Wever[2]

1 Department of Pharmacology & Therapeutics, Faculty of Medicine & Health Sciences, U. A. E. University, Al-Ain, United Arab Emirates, **2** Laboratory of Experimental Cancer Research, University Hospital, Gent, Belgium, **3** Coastside Bio Resources, Stonington, Maine, United States of America, **4** Division of Molecular Carcinogenesis, Center for Neurological Diseases and Cancer, Nagoya University Graduate School of Medicine, Nagoya, Japan, **5** Department of Physiology, Faculty of Medicine & Health Sciences, U. A. E. University, Al-Ain, United Arab Emirates

Abstract

A major challenge for oncologists and pharmacologists is to develop less toxic drugs that will improve the survival of lung cancer patients. Frondoside A is a triterpenoid glycoside isolated from the sea cucumber, *Cucumaria frondosa* and was shown to be a highly safe compound. We investigated the impact of Frondoside A on survival, migration and invasion *in vitro*, and on tumor growth, metastasis and angiogenesis *in vivo* alone and in combination with cisplatin. Frondoside A caused concentration-dependent reduction in viability of LNM35, A549, NCI-H460-Luc2, MDA-MB-435, MCF-7, and HepG2 over 24 hours through a caspase 3/7-dependent cell death pathway. The IC50 concentrations (producing half-maximal inhibition) at 24 h were between 1.7 and 2.5 μM of Frondoside A. In addition, Frondoside A induced a time- and concentration-dependent inhibition of cell migration, invasion and angiogenesis *in vitro*. Frondoside A (0.01 and 1 mg/kg/day i.p. for 25 days) significantly decreased the growth, the angiogenesis and lymph node metastasis of LNM35 tumor xenografts in athymic mice, without obvious toxic side-effects. Frondoside A (0.1–0.5 μM) also significantly prevented basal and bFGF induced angiogenesis in the CAM angiogenesis assay. Moreover, Frondoside A enhanced the inhibition of lung tumor growth induced by the chemotherapeutic agent cisplatin. These findings identify Frondoside A as a promising novel therapeutic agent for lung cancer.

Citation: Attoub S, Arafat K, Gélaude A, Al Sultan MA, Bracke M, et al. (2013) Frondoside A Suppressive Effects on Lung Cancer Survival, Tumor Growth, Angiogenesis, Invasion, and Metastasis. PLoS ONE 8(1): e53087. doi:10.1371/journal.pone.0053087

Editor: Srikumar P. Chellappan, H. Lee Moffitt Cancer Center & Research Institute, United States of America

Received June 13, 2012; **Accepted** November 27, 2012; **Published** January 8, 2013

Funding: This work was financially supported by the FMHS grant number NP/08/27 (SA), the UAE University grant under a contract no. 01-04-8-11/09 (SA), the Terry Fox Fund for Cancer Research (SA and TA), the UAEU-NRF 09/10 grant number 21MO72 (SA), and the Maine Technology Institute, Gardiner, Maine, USA, and the National Cancer Institute, RAPID Program (PC). The funding agencies had no role in study design, data collection and analysis, decision to publish, or preparation of the manuscript.

Competing Interests: Peter Collin is director, laboratory manager, employee and stock-holder of Coastside Bio Resources, a Maine, USA Corporation. Thomas Adrian and Peter Collin are co-inventors of a United States patent describing Frondoside A and other sea cucumber glycosides as putative anti-cancer agents, and may benefit financially if Frondoside A becomes a drug for human cancers. This does not alter the authors' adherence to all the PLOS ONE policies on sharing data and materials.

* E-mail: samir.attoub@uaeu.ac.ae

Introduction

Lung cancer is the most common form of cancer with one of the highest mortality rates in the world. Targeted therapies for selected subgroups of patients constitute a remarkable progress in the treatment of lung cancer. However, despite these advances, controversies remain, patients die, and a cure remains elusive [1]. Natural compounds are emerging as a new generation of anticancer agents with limited toxicity in cancer patients [2,3]. They can have high value in tumors resistant to classical chemotherapies or resistant to tyrosine kinase inhibitors such as gefitinib

Sea cucumbers have been valued for hundreds of years in the Chinese diet as a food delicacy, as well as a medicine for a wide variety of diseases. In the United States and Canada, sea cucumber tissues are dried, pulverized and encapsulated as nutraceuticals for over-the-counter dietary health supplements, primarily directed at inflammatory conditions in humans and companion animals [4]. Frondoside A is a triterpenoid glycoside isolated from the Atlantic cucumber, *Cucumaria frondosa*. (See [5] for chemical structure). Recent studies demonstrate that low concentrations of Frondoside A inhibit the growth and induced apoptosis of human pancreatic, leukemia and breast cancer cells via caspase activation [6–8].

The chemotherapeutic agents currently in use for lung cancer are still unsatisfactory due to associated co-lateral toxicity and drug-induced resistance [9–11] which motivate our investigation of the impact of Frondoside A on human non-small cell lung cancer survival, migration and invasion *in vitro*, and on tumor growth, metastasis and angiogenesis *in vivo* alone and in combination with cisplatin.

Materials and Methods

Cell culture and reagents

Human lung cancer cells LNM35 (NSCLC) [12], A549 and NCI-H460-Luc2 (Caliper LifeSciences, US) were maintained in RPMI 1640 (Invitrogen, Paisley, UK), human melanoma MDA-MB-435, human mammary adenocarcinoma cells MCF-7, and human hepatoma cells HepG2 were maintained in DMEM (Invitrogen, Paisley, UK). All media were supplemented with antibiotics (penicillin 50 U/ml; streptomycin 50 µg/ml) (Invitrogen, Cergy Pontoise, France) and with 10% fetal bovine serum (FBS, Biowest, Nouaille, France). EndoGRO^{TM} Human Umbilical Vein Endothelial Cells (HUVECs) (Millipore, Temecula, CA) were maintained in EndoGRO^{TM}-MV-VEGF Complete Media Kit (Millipore, Temecula, CA). Cisplatin was purchased from Sigma-Aldrich (Sigma-Aldrich, Saint-Quentin Fallavier, France). Frondoside A was purified from *Cucumaria frondosa*, harvested near Stonington, Maine and the purity (99.9%) confirmed by NMR as previously described [13,14].

Cellular viability

Cells were seeded at a density of 5,000 cells/well into 96-well plates. After 24 h, cells were treated for another 24 h with different concentrations of Frondoside A (0.01–5 µM), in triplicate. Control cultures were treated with 0.1% DMSO. The effect of Frondoside A on cell viability was determined using a CellTiter-Glo Luminescent Cell Viability assay (Promega Corporation, Madison, USA), based on quantification of ATP, which signals the presence of metabolically active cells. The luminescent signal was measured using the GLOMAX Luminometer system. Data were presented as proportional viability (%) by comparing the treated group with the untreated cells, the viability of which is assumed to be 100%.

Caspase 3/7 activity

LNM35 cells were seeded at the density of 5,000 cells/well into 96-well plate and treated with Frondoside A (1–2.5 µM) for 2 and 24 h, in triplicate. Caspase-3/7 activity was measured using a luminescent Caspase-Glo 3/7 assay kit following the manufacturer's instructions (Promega Corporation, Madison, USA). Caspase reagent was added and the plate was mixed using an orbital shaker and incubated for 2.5 h at room temperature. Luminescence was measured using a GLOMAX Luminometer system.

Wound healing motility assay

LNM35 cells were grown in six-well tissue culture dishes until confluence. Cultures were incubated for 10 min with Moscona buffer. A scrape was made through the confluent monolayer with a plastic pipette tip of 1 mm diameter. Afterwards, the dishes were washed twice and incubated at 37°C in fresh RPMI containing 10% fetal bovine serum in the presence or absence of the non-toxic concentrations of Frondoside A (0.1–0.5 µM). At the bottom side of each dish, two arbitrary places were marked where the width of the wound was measured with an inverted microscope (objective ×4) (Olympus 1X71, Japan). Motility was expressed as the average ± S.E.M of the difference between the measurements at time zero and the 6, 24 and 30 h time period considered.

Matrigel invasion assay

The invasiveness of the lung cancer cells LNM35 treated with Frondoside A (0.1–1 µM) was tested using BD Matrigel Invasion Chamber (8-µm pore size; BD Biosciences, Le Pont de Claix, France) according to manufacturer's protocol. The PI3 kinase inhibitor LY294002 (20 µM) was used as a positive inhibitor of cellular invasion. Briefly, Cells (1×10^5 cells in 0.5 mL of media and the indicated concentration of Frondoside A) were seeded into the upper chambers of the system, the bottom wells in the system were filled with RPMI supplemented with 10% fetal bovine serum as a chemo-attractant and then incubated at 37°C for 24 h. Non-penetrating cells were removed from the upper surface of the filter with a cotton swab. Cells that have migrated through the Matrigel were fixed with 4% formaldehyde, stained with DAPI and counted in 25 random fields under a microscope. The assay was carried out in duplicate and repeated three times for quantitative analysis.

Chorioallantoic membrane (CAM) angiogenesis assay

This assay was performed as described previously [15], with some modifications. Briefly, fertilized eggs were incubated for 3 days at 37, 8°C with a humidity of 48%. On day 4, albumen was removed to detach the shell from the developing CAM and a window was made in the eggshell, exposing the CAM, and covered with a breathing film (suprasorb F®). The eggs were returned to the incubator until day 10, prior to application of the test compounds. Test compound and control compound (DMEM without 10% FBS) dissolved in DMEM without 10% FBS were poured onto separate sterile discs (12 mm diameter), which were allowed to dry under sterile conditions. A solution of cortisone acetate (125 µg/disc) was poured onto all discs to prevent an inflammatory response. Test discs probed with recombinant human bFGF (Peprotech) served as a control for angiogenesis stimulation. On each CAM, the disc containing control compound and the disc containing test compound were placed at a distance of 1 cm. The windows were covered and the eggs were incubated until day 14, before assessment of angiogenesis. Therefore, the eggs were flooded with 10% buffered formalin and the eggs were kept at room temperature for at least 20 minutes. The CAM, the area of the discs included, was placed in a petri dish with 10% buffered formalin. The plastic discs were removed and phase-contrast pictures of the area of the plastic discs were taken. The vascular index was measured as described previously [16]. Vascular intersections on a grid containing three concentric circles (6, 8 and 10 mm diameter with as center the center of the disc) were counted. The angiogenic index = $(t-c)/c$, with t the number of intersections in the area covered by the test disc and c the number of intersections in the area covered by the control disc in the same egg. The Mann-Whitney U-test was used for statistical analysis ($p<0.05$).

Vascular tube formation assay

Assessment of *in vitro* capillary formation used Matrigel (Becton Dickinson, Le Pont de Claix, France). Matrigel is a squamous cell carcinoma basement membrane matrix composed primarily of collagen IV, laminin, entactin, and heparan sulfate proteoglycans. The Matrigel matrix was thawed, gently mixed to homogeneity using cooled pipettes, and diluted v/v with the EndoGRO^{TM}-MV-VEGF Complete Media Kit medium (Millipore, Temecula, CA, USA). Matrigel, 50 µl/well, supplemented with angiogenic peptides and other effectors was used to coat the wells of 96-well plates. The plate was then incubated for one hour at 37°C to allow the matrix solution to solidify prior to treatment. HUVECs (at a density of about 4×10^4 cells/well and the indicated concentration of Frondoside A) were plated to each well and incubated for 8 h at 37°C in 0.1 mL of EndoGRO^{TM}-MV-VEGF Complete Media Kit medium (Millipore, Temecula, CA, USA). Then cells were photographed using an inverted phase contrast photomicroscope. The tubular network growth area was compared in control and inhibitor-treated Matrigel matrix. Tube formation was quantified by counting the number of tube-like structures formed in each

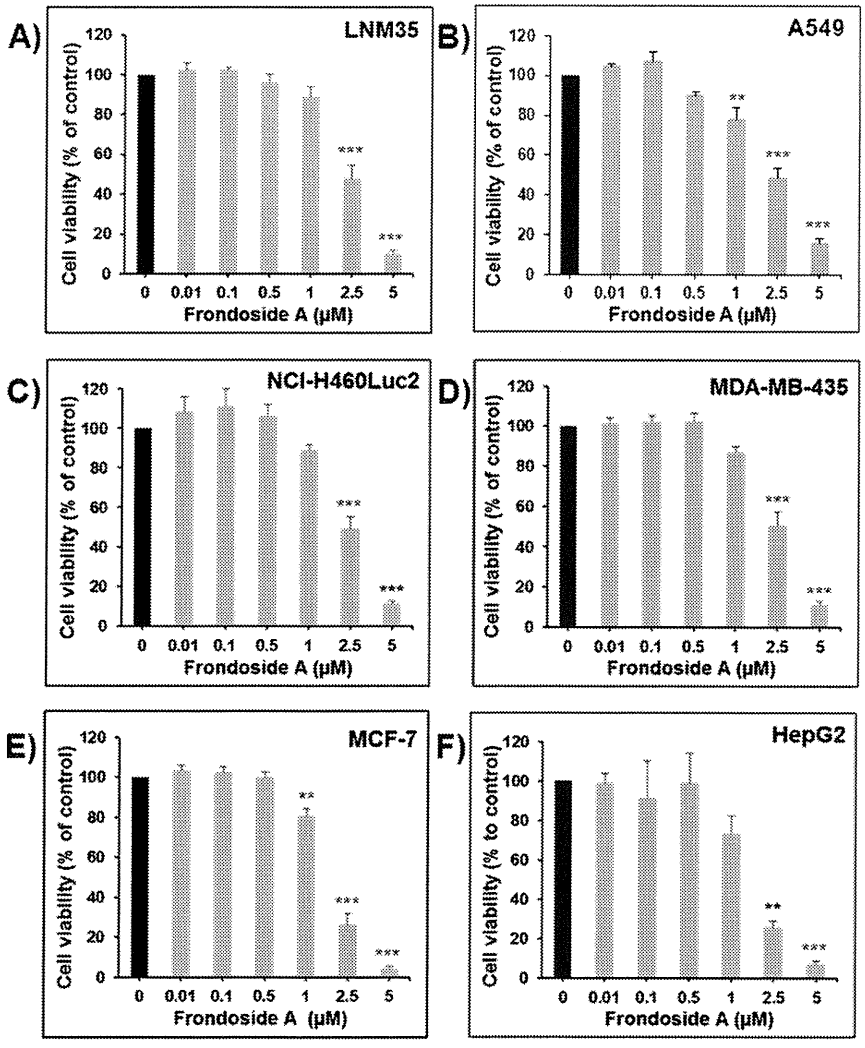

Figure 1. Inhibition of cellular viability by Frondoside A. Exponentially growing LNM35 (**A**), A549 (**B**), NCI-H460-Luc2 (**C**), MDA-MB-435 (**D**), MCF-7 (**E**), and HepG2 (**F**) cells were treated with vehicle (0.1% DMSO) and the indicated concentrations of Frondoside A. Viable cells were assayed as described in Materials and Methods. All experiments were repeated at least three times. *Columns*, mean; *bars*, S.E.M. **Significantly different at $P<0.01$, ***Significantly different at $P<0.001$.
doi:10.1371/journal.pone.0053087.g001

well. The effect of Frondoside A on viability of the HUVEC was determined using a CellTiter-Glo Luminescent Cell Viability assay (Promega Corporation, Madison, USA), as previously described for the cancer cells.

Tumor growth and metastasis assay

The animal experiments were performed in accordance with the protocol approved by the animal ethics committee and the Institutional Animal Care at the Faculty of Medicine & Health Sciences/UAE University. Six-week-old athymic NMRI female nude mice (nu/nu, Charles River, Germany) were housed in filtered-air laminar flow cabinets and handled under aseptic conditions. Procedures involving animals and their care were conducted in conformity with Institutional guidelines that are in compliance with Faculty of Medicine & Health Sciences, national and international laws and policies (EEC Council Directive 86/609, OJ L 358, 1, December 12, 1987; and NIH Guide for Care and Use of Laboratory Animals, NIH Publication No. 85-23, 1985). LNM35 cells (1×10^6 cells in 200 μl PBS) were injected subcutaneously into the lateral flank of the nude mice. One week

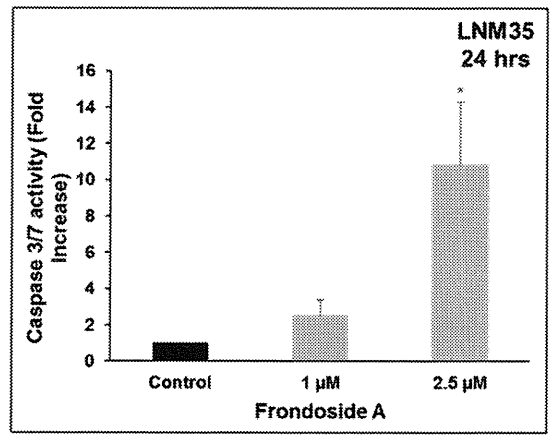

Figure 2. Induction of caspase-3/7 activity was analyzed in LNM35 cells treated for 24 h with Frondoside A (1–2.5 μM), normalized to the number of viable cells per well and expressed as fold induction compared with the control group. *Significantly different at $P<0.05$.
doi:10.1371/journal.pone.0053087.g002

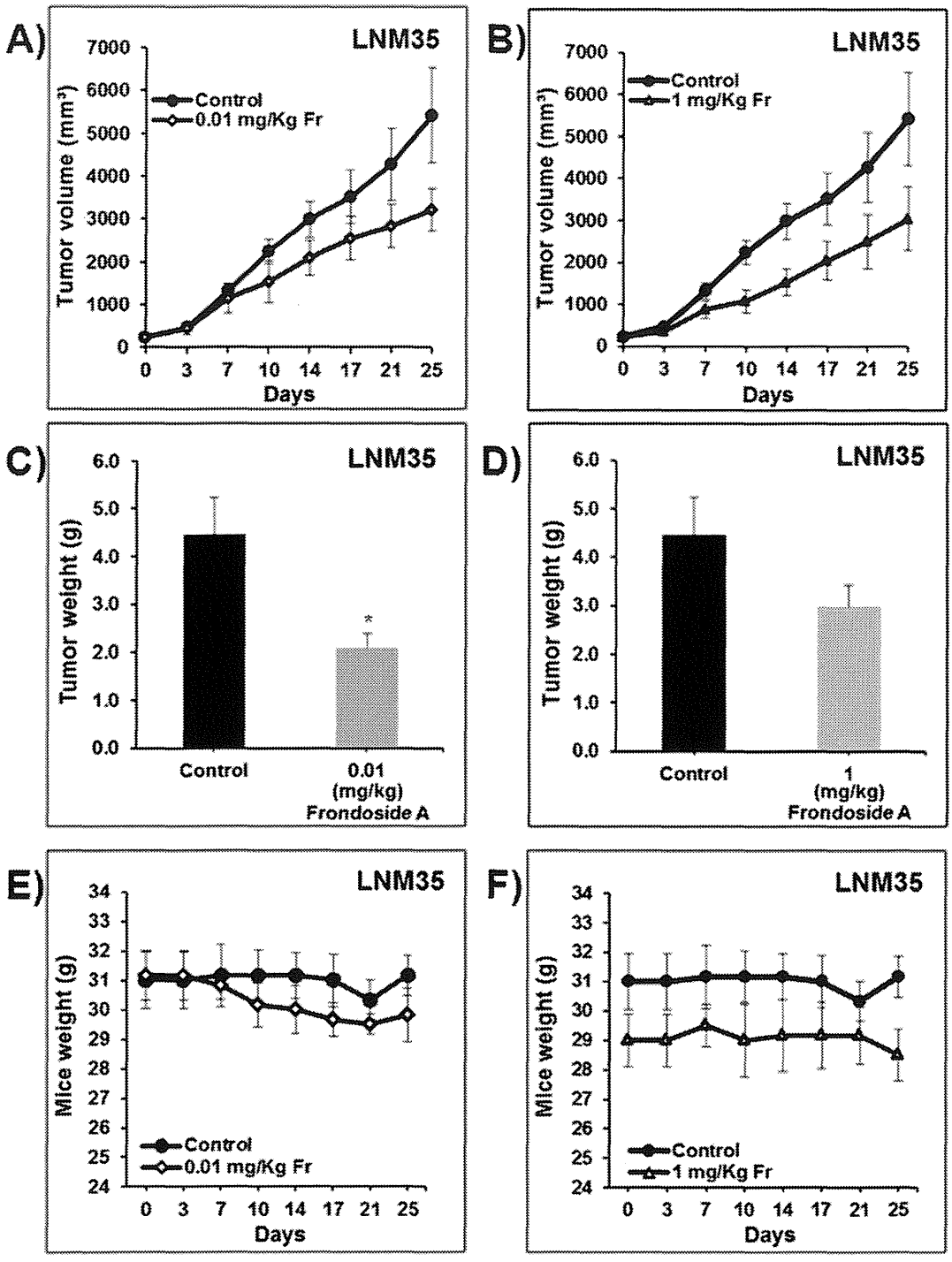

Figure 3. Frondoside A induces regression of established LNM35 xenografts. A) & B) Tumor volume of LNM35 xenografts inoculated subcutaneously in nude mice and treated with Frondoside A (0.01 and 1 mg/kg, intra-peritoneal injections, respectively) or control carrier solution alone, for a total of 25 days. Data points represent the mean ± S.E.M. of 6 mice per group. **C) & D**) Tumor weight obtained from the same control and treated nude mice. Data points represent the mean ± S.E.M. of 6 mice per group. *Columns*, mean; *bars*, S.E.M. **E) & F**) Body weight of these mice. Data points represent the mean ± S.E.M. of 6 mice per group. *Significantly different at $P<0.05$.
doi:10.1371/journal.pone.0053087.g003

after inoculation, when tumors had reached the volume of approximately 150 mm^3, animals (six in each group) were treated in the first protocol for 25 days with Frondoside A (0.01 and 1 mg/kg/day, ip) or carrier solution (control) in order to determine the effect of Frondoside A alone on tumor growth and metastasis. In the second protocol, animals were treated for only 10 days with the lowest dose of Frondoside A (0.01 mg/kg/day, ip), cisplatin (1 mg/kg/day, ip), or with combined Frondoside A and cisplatin treatment. Control animals were treated with carrier solution. Tumor dimensions and animal weights were

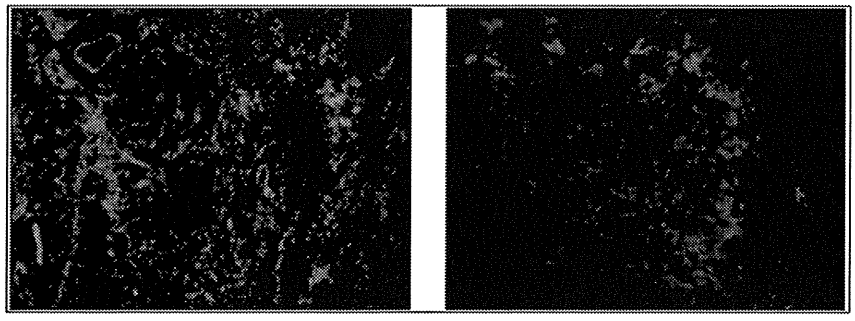

Figure 4. The anti-angiogenic activity of Frondoside A in the xenograft tumor: Immuno-histochemical staining of lung xenograft tumors for CD31 (microvessel density).
doi:10.1371/journal.pone.0053087.g004

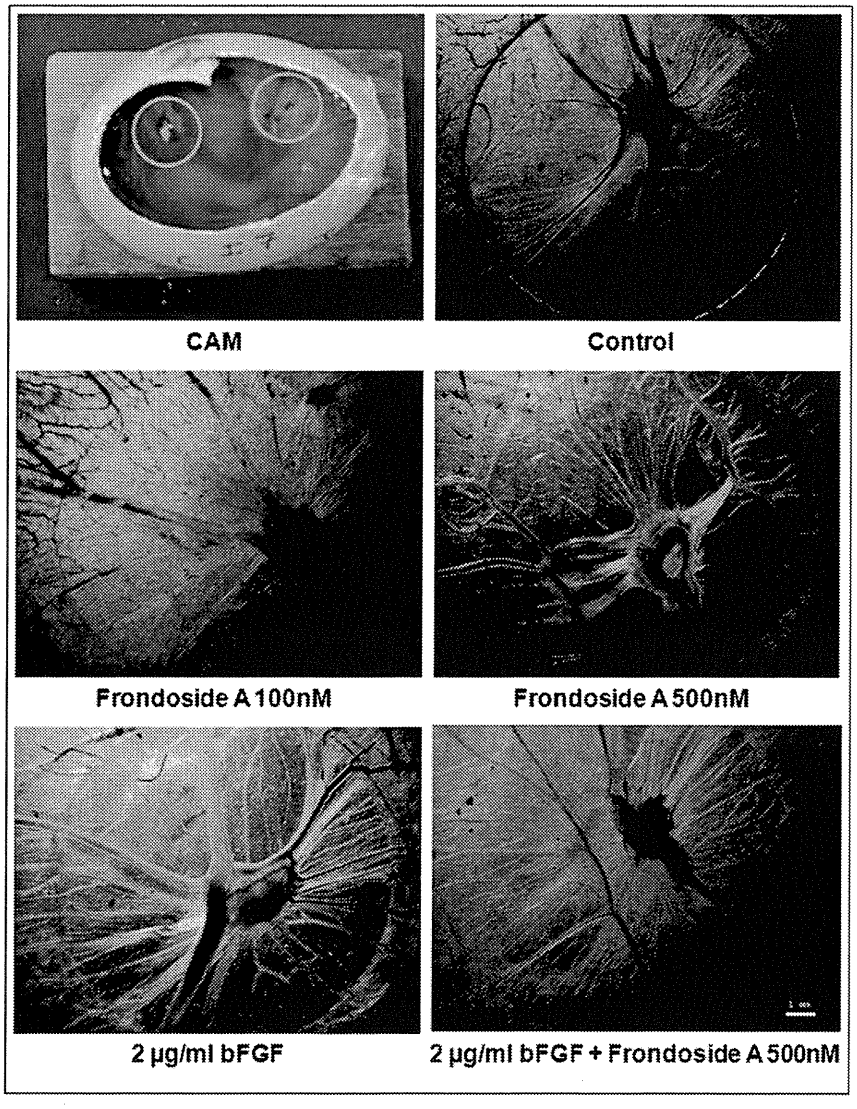

Figure 5. The anti-angiogenic activity of Frondoside A in the Chorioallantoic membrane (CAM) assay *in vivo*: CAM was treated with control (serum-free medium), 100 nM Frondoside A, 500 nM Frondoside A, 2 µg/mL bFGF, 2 µg/mL bFGF+500 nM Frondoside A and the vascularization of test discs was photographed.
doi:10.1371/journal.pone.0053087.g005

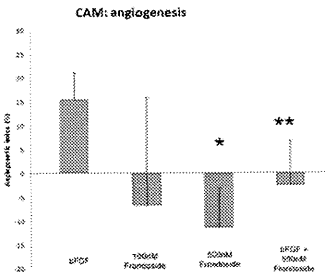

Figure 6. Quantification of CAM angiogenesis assay: *Bars* indicate angiogenic indices (%) of CAM's probed with 2 μg/mL bFGF, 100 nM Frondoside A, 500 nM Frondoside A, 2 μg/mL bFGF+500 nM Frondoside A. Data represents mean ± SD (Mann-Whitney U-test, *: $p<0.05$, ***: $p<0.01$). In each experiment, six eggs were tested per condition.
doi:10.1371/journal.pone.0053087.g006

measured every 3 days. Tumor volume (V) was calculated using the formula: $V = 0.4 \times a \times b^2$, with "a" being the length and "b" the width of the tumor. After sacrifice, the tumors and axillary lymph nodes were excised and weighed.

Immuno-histochemical determination of CD31/platelet-endothelial cell adhesion molecule 1 (PECAM-1) for Microvessel Density

The effect of Frondoside A on angiogenesis was evaluated using CD31 immuno-staining. The tumor tissues were quickly frozen in isopentane at −130°C and stored at −70°C until further processing. Eight-μm frozen sections were fixed in acetone, and incubated overnight with a CD31 antibody (clone MEC13.3, 1:100) (BD Pharmingen, San Jose, CA, USA). Slides were then washed three times in PBS and incubated with secondary antibody labeled with rhodamine (goat anti-rat 1:100) for one hour at room temperature. The area occupied by CD31-positive microvessels and total tissue area per section were compared between treated and control mice. All analyses were performed in a blind fashion.

Results were expressed as means ± S.E.M. of the number of experiments. The difference between experimental and control values were assessed by ANOVA followed by Dunnett's post-hoc multiple comparison test. Tumor growth and metastasis studies were analyzed using the unpaired Student's t-test. $P<0.05$ indicate a significant difference.

Results

Effect of Frondoside A on cellular viability

As shown in **fig. 1**, Frondoside A concentrations (0.01–5 μM) caused a concentration-dependent decrease in cell viability of LNM35, A549, NCI-H460-Luc2, MDA-MB-435, MCF-7, and HepG2 cells over 24 hours. The IC50 concentrations (producing half-maximal inhibition) at 24 h were in the range of 1.7 and 2.5 μM Frondoside A for all cell lines.

Frondoside A induces caspase-3/7 activation

Caspase-3/7 activity is essential in apoptotic cell death pathways. The relative activity of caspases 3/7 was analyzed in LNM35 cells treated for 2 and 24 h with Frondoside A (1–2.5 μM), and normalized to the number of cells per well. As shown in **Fig. 2**, caspase 3/7 activity increased by 2.5- and 10.8-fold in LNM35 cells treated for 24 h with Frondoside A 1 and 2.5 μM respectively. Similar effect was observed after treatment with Frondoside A (1–2.5 μM) for 2 h (data not shown).

Impact of Frondoside A on LNM35 xenografts

To confirm the pharmacological relevance of our *in vitro* data, the anticancer activity of Frondoside A was investigated *in vivo* in athymic mice inoculated with LNM35 lung cancer cells. The growth of the LNM35 human tumor xenografts was monitored every third or fourth day for 25 consecutive days after daily i.p. injection of 0.01 mg and 1 mg/kg of Frondoside A. Treatment with the lowest dose of Frondoside A (0.01 mg/kg/day) reduced the volume of the LNM35 xenografts by 41% (**Fig. 3A**). A similar difference was also found in tumor weight at the end of the experiment (2.1+/−0.3 g versus 4.5+/−0.8 g; $P<0.05$; **Fig. 3C**). Treatment with the highest dose (100 times more) of Frondoside A (1 mg/kg/day) reduces about 43.9% tumor volume of the LNM35 xenografts (**Fig. 3B**). Almost similar difference was found in tumor weight at the end of the experiment (3+/−0.5 g versus 4.5+/−0.8 g; **Fig. 3D**). This experiment clearly demonstrated that the lowest dose of Frondoside A (0.01 mg/kg/day) is optimal for the inhibition of tumor growth. There were no manifest undesirable effects of Frondoside A treatment on animal behaviour or body weight in either experiment (**Fig. 3E and 3F**). In addition, there were no visible abnormalities at necropsy, or any other obvious signs of toxicity as previously described by our team [**7**].

Inhibition of angiogenesis by Frondoside A in the xenografted tumors and the CAM assay *in vivo* and in the capillary-like structures *in vitro*

Angiogenesis is an attractive target in cancer therapy not only because it supplies oxygen and nutrients for the survival of tumor cells but also provides the route for metastatic spread of these cancer cells. First, we demonstrate that in the proliferating areas at the periphery of the tumor, microvessel density (measured by CD31 staining) was significantly reduced by Frondoside A (0.01 mg/kg/day) (**Fig. 4, right panel**) in comparison with the control-treated tumors (**Fig. 4, left panel**). Next, we used the CAM assay involving the coordination and integration of multicellular responses during development of the chick embryo to confirm this potential anti-angiogenic effect of Frondoside A. As shown in **Fig. 5 and 6**, bFGF (2 μg/ml), stimulated 15% new vessel formation with angiogenic indices statistically different compared with the control DMEM medium. Frondoside A (100 and 500 nM) inhibited basal angiogenesis in a concentration-dependent manner with respectively 7% and 12% inhibition of angiogenic index compared to control (**Fig. 5 and 6**). The formation of new blood vessels induced by bFGF was also completely suppressed by Frondoside A (500 nM) (**Fig. 5 and 6**). Finally, to assess whether the anti-angiogenic effect of Frondoside A involves a direct interaction of the compound with endothelial cells, we conducted comparative studies on the formation of capillary-like structures *in vitro*, using HUVECs plated on Matrigel-coated plates. As shown in **Fig. 7A**, human endothelial cells have the ability to form capillary structures when seeded and cultured on top of Matrigel substrate. Control cells move from their initial uniform pattern of dispersed cell layers and associate to form a network of cell clusters connected by long, multicellular processes leading to the formation of tube-like structures. Addition of non-toxic concentrations of Frondoside A (0.01–1 μM) resulted in a marked inhibition of this spontaneous angiogenic phenotype (**Fig. 7A, and 7B**). Frondoside A induced inhibition of this spontaneous angiogenic phenotype occurred without significant reduction of cell viability (**Fig. 7C**). Taken together, these data confirm a strong anti-angiogenic potential of Frondoside A.